HHS Public Access

Author manuscript

Phys Med Biol. Author manuscript; available in PMC 2016 May 21.

Published in final edited form as:

Phys Med Biol. 2015 May 21; 60(10): 3999–4013. doi:10.1088/0031-9155/60/10/3999.

Risk-optimized proton therapy to minimize radiogenic second cancers

Laura A. Rechner[1,2,3], **John G. Eley**[1,2], **Rebecca M. Howell**[1,2], **Rui Zhang**[1,2,4], **Dragan Mirkovic**[1,2], and **Wayne D. Newhauser**[1,2,4,5,6]

[1]The University of Texas Health Science Center Houston, Graduate School of Biomedical Sciences, Houston, TX 77030, USA

[2]Department of Radiation Physics, The University of Texas MD Anderson Cancer Center, 1515 Holcombe Boulevard, Houston, TX 77030, USA

[3]Present Address: Department of Radiation Oncology, Rigshospitalet, Blegdamsvej 9, 2100 København Ø, Denmark

[4]Department of Physics and Astronomy, Louisiana State University, 202 Nicholson Hall, Baton Rouge, LA 70803, USA

[5]Department of Medical Physics, Mary Bird Perkins Cancer Center, 4950 Essen Lane, Baton Rouge, LA 70809, USA

Abstract

Proton therapy confers substantially lower predicted risk of second cancer compared with photon therapy. However, no previous studies have used an algorithmic approach to optimize beam angle or fluence-modulation for proton therapy to minimize those risks. The objectives of this study were to demonstrate the feasibility of risk-optimized proton therapy and to determine the combination of beam angles and fluence weights that minimize the risk of second cancer in the bladder and rectum for a prostate cancer patient. We used 6 risk models to predict excess relative risk of second cancer. Treatment planning utilized a combination of a commercial treatment planning system and an in-house risk-optimization algorithm. When normal-tissue dose constraints were incorporated in treatment planning, the risk model that incorporated the effects of fractionation, initiation, inactivation, and repopulation selected a combination of anterior and lateral beams, which lowered the relative risk by 21% for the bladder and 30% for the rectum compared to the lateral-opposed beam arrangement. Other results were found for other risk models.

Keywords

second cancer; proton therapy; risk optimization; prostate cancer

[6]Author to whom any correspondence should be addressed newhauser@lsu.edu.

The authors do not report any conflicts of interest.

1. Introduction

Improvements in cancer detection and treatment have led to increased survival rates. In the United States, the 5-year survival rate for all cancers has increased from about 50% (1975-1977) to 68% (2003-2009) (Siegel *et al* 2014). It is estimated that there are 14.5 million cancer survivors in the US and this number is expected to increase to nearly 19 million by 2024 (Desantis *et al* 2014). Because of the increasing population of long-term survivors, minimizing the risk of treatment-related late effects, such as the development of a radiogenic second cancer (Followill *et al* 1997, Verellen and Vanhavere 1999, Friedman *et al* 2010, Berrington de Gonzalez *et al* 2011, Newhauser and Durante 2011, NCRP 2011), has become increasingly important.

Considerable attention has been paid to quantifying and reducing the risk of late effects following radiotherapy (Newhauser and Durante 2011, NCRP 2011). For example, the use of proton therapy has been shown to reduce the predicted risk of late effects of radiotherapy (Brodin *et al* 2011), including the development of a second cancer (Miralbell *et al* 2002, Mu *et al* 2005, Schneider *et al* 2006, Fontenot *et al* 2009, Newhauser *et al* 2009, Taddei *et al* 2010, Rechner *et al* 2012, Arvold *et al* 2012, Efstathiou *et al* 2012, Moteabbed *et al* 2014), cardiac toxicity (Zhang *et al* 2013) and fertility complications (Pérez-Andújar *et al* 2013) relative to the corresponding risks after photon radiotherapy. In addition, it has been shown that in-field or field-bordering organs are the largest contributing factor when predicting or measuring the risk of second cancer after external beam radiotherapy for the prostate (Fontenot *et al* 2009, 2010) and for childhood cancers (Diallo *et al* 2009), including the craniospinal axis (Newhauser *et al* 2009). For these reasons, it appears that second cancer risks could be substantially reduced by developing treatment planning strategies for proton therapy that minimize the predicted risk to in-field and field-bordering organs. One study optimized the prescription dose to minimize life years lost following radiotherapy for medulloblastoma patients by balancing the risk of tumor recurrence and side effects from treatment (Brodin *et al* 2014). However, to our knowledge, the literature contains no reports of optimization of beam angle or fluence modulation to specifically minimize the predicted risk of second cancer for a fixed prescription dose. Therefore, the feasibility and impact of risk-optimized treatment planning was previously unknown.

The aim of this work was to determine whether risk-optimized proton therapy (ROPT) is feasible and to minimize the predicted risk of second cancer in the bladder and rectum for a representative prostate cancer patient. To accomplish this aim, we applied risk models from the literature to patient-specific dosimetric data from a commercial treatment planning system (TPS) and Monte Carlo simulations. Additionally, we developed a risk-optimized treatment planning technique for ROPT that optimized proton fluence weights for each of 16 coplanar treatment beam orientations.

2. Methods and materials

2.1 Patient selection and organs at risk

The medical record for a 56-year-old prostate cancer patient was selected for use in this study. Data were collected in accordance with a protocol that was approved by The

University of Texas MD Anderson Cancer Center's (MDACC) institutional review board. The patient previously underwent proton therapy at MDACC for intermediate stage adenocarcinoma and is representative of the typical prostate cancer patient seen in our practice. The patient selected for this work was studied previously (Fontenot *et al* 2009, Rechner *et al* 2012), facilitating direct comparisons with those previous works. During CT simulation and treatment, a water filled balloon was inserted into the patient's rectum to immobilize the prostate and provide posterior rectal sparing. The clinical target volume (CTV) included the prostate and proximal seminal vesicles.

In a previous study, Fontenot *et al* (2009) reported that the predicted risk of second cancers in the bladder and rectum contribute most of the overall predicted risk of developing second cancers following proton radiotherapy for prostate cancer. Therefore, we considered the bladder and the rectum as organs at risk in this study. For purposes of risk prediction, we included the bladder wall and rectal wall and excluded their contents in accordance with the recent recommendations of the International Commission on Radiological Protection Publication 110 (2008).

2.2 Treatment planning and risk optimization

Initial treatment planning was completed using a commercial TPS (Eclipse version 9, Varian Medical Systems, Palo Alto, CA, USA) that was clinically commissioned for proton therapy (Newhauser *et al* 2007). 16 passively-scattered proton beams were placed at equal intervals of gantry angle separation around the patient. Lateral, proximal, and distal margins for each beam were defined using the methodology described in the literature (Moyers *et al* 2001) and used for prostate treatment planning at our institution. Beam angles started at 0 degrees and were placed at intervals of 22.5 degrees. The individual beams were designed such that one beam, and any combination thereof, provided uniform coverage of the treatment volume. The prescribed RBE-weighted absorbed dose was 76 Gy (RBE), where absorbed dose in Gy was weighted by a generic relative biological effectiveness (RBE) of 1.1 following the recommendations of the International Commission on Radiation Units and Measurements (2007). Note that for the purposes of this study, namely combining exposures from therapeutic proton beams and leakage neutrons, we expressed the therapeutic dose in Gy (RBE) as numerically equivalent to the radiation protection quantity equivalent dose in Sv. For prescribing doses and evaluating therapeutic aspects of treatment plans, we followed the recommendations of the International Commission on Radiation Units and Measurements (2007) regarding quantities and units.

For each beam of the 16 therapeutic proton beams, the stray neutron dose contributions were calculated with Monte Carlo simulations (Rechner *et al* 2012). Neutron absorbed doses were converted from Gy to equivalent dose in Sv by applying a mean radiation weighting factor of 10 based on results from previous studies (Zheng *et al* 2008).

Dose matrices containing primary and stray radiation were exported from the TPS and Monte Carlo output files and imported into an in-house code for processing (MATLAB version R2013a, Mathworks, Natick, MA). Processing included summing the proton doses and neutron equivalent doses on a voxel-byvoxel basis to produce a total equivalent dose

matrix for each gantry angle. These matrices served as input data for the risk optimization algorithm.

The risk optimization method used in this study was implemented in an in-house code and searched over all possible searched over all possible combinations in the set where beam weights are positive and sum to 1. Additionally, because of the symmetry of the pelvis, corresponding left and right beams (at the same angle from 0 degrees) conferred virtually identical risk. Therefore, corresponding left and right beams (with the exception of the anterior-posterior and posterior-anterior beams, which did not have corresponding beams) were constrained to equal one another. The magnitude of relative beam weight variation was discretized to 0.1 (or 0.05 for each beam in a left/right beam pair). As the algorithm searched over all combinations, the combination with the lowest risk found yet was flagged as the provisional best permutation. Additionally, the code tested whether the dose volume histogram (DVH) constraints used clinically at our institution were met (table 1). Once all combinations were examined, the best two ROPT plans for each risk model were flagged for further analysis, namely, the plans that only minimized predicted risk, and those that minimize predicted risk and satisfied the DVH constraints.

To calculate the excess relative risk for second cancer induction after radiotherapy for each tissue (ERR_T) for each solution of beam weight combinations, we applied a risk model that accounts for initiation, inactivation, repopulation, and promotion (*iirp*), and the effects of fractionation (Sachs and Brenner 2005, Shuryak *et al* 2009b, 2009a, 2011). This model integrates both long- and short-term models. The stochastic short-term model considers the number of microenvironments called stem cell niches that can be eradicated or initiated to become pre-malignant. The long-term model assumes that stem cells are located in these tissue niches, that an initiated stem cell either dies out or initiates a whole niche (i.e., forming a premalignant clone), that pre-malignant cells lose carcinogenic potential with age, and that there is a net proliferation rate of premalignant niches. The *iirp* risk model was compiled from two related manuscripts and an erratum (Shuryak *et al* 2009b, 2009a, 2011) and ERR_T was calculated by

$$ERR_{T}=\sum_{i=1}^{N}\left[\frac{V_i}{V_T}\times\left(\left(\left(Q_1\left(i\right)Q_2\left(i\right)+Q_3\right)/Q_4\right)-1\right)\right], \quad (1)$$

where V_i is the volume of the ith voxel (out of N voxels) and V_T is the total organ volume. The term Q1 describes the promotion of existing premalignant stem-cell niches by radiation and a subsequent loss of carcinogenic potential with time. The term Q2 models the number of healthy stem cells initiated by radiation, including effects of repopulation and inactivation during fractionated radiotherapy. Parts Q3 and Q4 model the proliferation of radiation-induced and existing (background) premalignant niches, respectively. The terms Q_1 through Q_4 are defined as

$$Q_1\left(i\right)=\left(1+YD\left(i\right)\right)/\left(1+YD\left(i\right)\left(1-exp\left(-\delta T_y\right)\right)\right), \quad (2)$$

$$Q_2\left(i\right)=\left(\left(exp\left(bT_x\right)-1\right)S_f\left(Z,D\left(i\right)\right)+bXI_{sf}\left(D\left(i\right)\right)\right)exp\left(bT_y\right), \quad (3)$$

$$Q_3 = exp\left(bT_y\right) - 1, \quad \text{and} \quad (4)$$

$$Q_4 = exp\left(b\left(T_x + T_y\right)\right) - 1. \quad (5)$$

In equation 3 I_{Sf}(D(i)) represents the net outcome of initiation, inactivation, and cell repopulation during radiation exposure, and S_f(Z,D(i)) represents the probability that a pre-existing pre-malignant stem cell niche survives irradiation. I_{Sf}(D(i)) and S_f(Z,D(i)) were calculated according to the stochastic methods described in the manuscripts from Shuryak *et al* (2009a, 2011). For a full description of the stochastic part of the risk model, the reader is referred to the references listed above; however, the equations are also listed below:

$$I_{Sf}\left(D\left(i\right)\right) = \sum_{k=1}^{K} I\left(i,k\right) F\left(i,k\right) \quad \text{and} \quad S_f\left(D\left(i\right)\right) = 1 - \left(1 - F\left(0\right)\right)^Z, \quad \text{where} \quad (6)$$

the term $I(i,k)$ helps to describe the number of cells initiated and is given by

$$I\left(i,k\right) = d\left(i\right) n^+\left(i,k\right) / \nu, \quad (7)$$

the clone survival probability is given by

$$F\left(i,k\right) = \frac{1}{\Delta\left(i,k\right)}, \quad (8)$$

the term $\Delta(i,k)$ is given by

$$\Delta\left(i,k\right) = 1 + \sum_{j=k+1}^{K} \frac{1 - S\left(i,j\right)}{\prod_{m=k}^{j-1} R\left(i,m\right) S\left(i,m+1\right)}, \quad (9)$$

the ratio of stem cells after a radiation fraction to before a radiation fraction is given by

$$R\left(i,k\right) = \frac{n^-\left(i,k+1\right)}{n^+\left(i,k\right)}, \quad (10)$$

the number of stem cells after a radiation fraction is given by

$$n^-\left(i,k+1\right) = \frac{n^+\left(i,k\right)\nu}{n^+\left(i,k\right) + \left(\nu - n^+\left(i,k\right)\right) exp\left(-\lambda\left(T\left(k+1\right) - T\left(k\right)\right)\right)}, \quad (11)$$

the number of stem cells before a radiation fraction is given by

$$n^+\left(i,k\right) = S\left(i,k\right) n^-\left(i,k\right), \quad \text{and} \quad (12)$$

the surviving fraction of cells is after a given radiation dose is given by

$$S\left(i,k\right) = exp\left(-\alpha d\left(i,k\right) - \beta d(i,k)^2\right). \quad (13)$$

In equations 1-13 the index *i* denotes the voxel, and the index *k* denotes the fraction. The definitions and values used in equations 6-13 can be found in table 2. In addition, we assumed that radiation exposure would not reduce the risk of second cancer relative to the unexposed population and constrained the *iirp* risk model to have a minimum of 0. Additionally, in order to span the different possible relationships between dose and risk, we applied the linear-non-threshold risk model (NRC 2006) and 4 other non-linear risk models (Lindsay *et al* 2001, Davis 2004, Sachs and Brenner 2005, Zheng *et al* 2008, Schneider and Walsh 2008, Shuryak *et al* 2009b, 2009a, Schneider *et al* 2011, Fontenot *et al* 2009, Rechner *et al* 2012). Of those 4 non-linear risk models, the first two models describe a linear-exponential relationship where after a specified maximum risk the risk decreases exponentially. The other two non-linear risk models demonstrate a linear-plateau relationship, where after the maximum risk the risk remains constant with increasing dose. For both the linear-exponential and the linear-plateau risk relationships, a low and a high dose for maximum risk were chosen, namely, 10 Sv and 40 Sv (expressed as linear-exponential-x and linear-plateau-x, where x denotes the numeric value of maximum risk). For all risk models, an exposed age of 60 years and attained age of 70 years was assumed. For these 5 risk models, the formula used to calculate ERR_{T} was

$$ERR_{\mathrm{T}}=f_{\mathrm{T}}\sum_{i=1}^{n}\left[\frac{V_i}{V_{\mathrm{T}}}\times R\right] \quad (14)$$

where the subscript T denotes the tissue of interest (bladder or rectum), *n* is the number of voxels in the tissue, f_{T} is the fractional mass of the subregion of interest compared to the total mass of the organ for which a risk coefficient is defined (0.2 for the rectum as a fraction of the whole colon, and 1 for the bladder since the whole bladder was considered) (Rechner *et al* 2012), V_i is the volume of the i^{th} voxel, and V_{T} is the volume of the tissue. *R* is the risk in the i^{th} voxel in tissue T and is alternately defined as

$$R=\mu_{\mathrm{T}}\times H_{\mathrm{i}} \quad \text{for the linear-non-threshold risk model,} \quad (15)$$

$$R=\mu_{\mathrm{T}}\times H_i\times e^{-\alpha_{\mathrm{T}}H_i} \quad \text{for the linear-exponential risk model, and} \quad (16)$$

$$R=\frac{\mu_{\mathrm{T}}}{\alpha_{\mathrm{T}}}\times\left(1-e^{-\alpha_{\mathrm{T}}H_i}\right) \quad \text{for the linear-plateau risk model.} \quad (17)$$

H_{i} is the equivalent dose (Sv) for the given voxel, and for the linear-non-threshold risk model μ_{T} is the tissue-specific risk coefficient (NRC 2006). For the non-linear risk models, the combination of the parameters μ_{T} and α_{T} control the shape of the curve, approximating the linear-non-threshold model at low doses and determining the dose level for maximum risk (10 Sv or 40 Sv in this study) (Fontenot *et al* 2009, 2010). Values for these coefficients are listed in table 3. In this study it was assumed that minimizing the values of ERR_{bladder} and ERR_{rectum} were of equal importance during optimization.

3. Results

Two ROPT treatment plans were created for each risk model, one with and one without consideration of DVH constraints, for a total of 12 optimized scenarios, of which 4 were unique (referred to as plans A, B, C and D, figure 1). All ROPT treatment plans provided clinically adequate coverage of the CTV, where 100% of the CTV received at least the prescribed dose of 76 Sv.

The ROPT treatment plan for the *iirp* risk model consisted of single posterior beam when DVH constraints were ignored (plan B, figure 1) and consisted of a heavily-weighted anterior beam and a small contribution from a lateral parallel-opposed pair when DVH constraints were respected (plan C, figure 1). This anterior plus lateral ROPT treatment plan (plan C) reduced the *ERR* by 21% for the bladder and 30% for the rectum when compared with the standard of care parallel-opposed treatment plan using the *iirp* risk model. Details of the ROPT plans are listed in tables 4 and 5.

For the linear-non-threshold model, the variation in ERR_{bladder} and ERR_{rectum} were plotted against beam angle (figure 2). The right-left-averaged values are plotted between 0 and 180 degrees for visual clarity. The value of ERR_{bladder} generally *decreased* as the beam angle increased from 0 to 180 degrees (from anterior to posterior), whereas the value of ERR_{rectum} generally *increased* as the beam angle increased from 0 to 180 degrees. It should be noted that this type of illustration is applicable only for the linear-non-threshold risk model, where the linear nature of the model allows the risk from any combination of beam angles to be found by calculating a weighted average of the risk contributions from each individual beam. The ROPT treatment plan that minimized second cancer in the bladder and rectum using the linear-non-threshold model consisted of a lateral parallel-opposed beam pair (plan A). The result did not change when DVH constraints were applied during optimization.

When the linear-exponential-10 risk model was used, the minimum *ERR* was achieved with a posterior beam (plan B), but when DVH constraints were applied, the lowest *ERR* was achieved by a heavily-weighted anterior beam and a small contribution from a lateral parallel-opposed pair (plan C). This result is qualitatively the same as the result found with the *iirp* risk model. When compared with the standard of care parallel-opposed treatment plan, the ROPT plan (plan C) reduced the risk of second cancer in the bladder by 19% and the rectum by 34% for the linear-exponential-10 risk model, while meeting normal tissue DVH constraints. For both the linear-exponential-40 and the linear-plateau-10 risk models, the ROPT plan was a pair of posterior-oblique beams (plan D); however, this plan did not meet the DVH constraints. When DVH constraints were included, the ROPT plan selected for the linear-exponential-40 and linear-plateau-10 risk models was a lateral parallel-opposed beam pair (plan A). For the linear-plateau-40 risk model, the ROPT plan was a lateral parallel-opposed beam pair (plan A), which met the DVH constraints. Summaries of all ROPT treatment plans are listed in tables 4 and 5.

4. Discussion and conclusion

In this study, we demonstrated the feasibility of including a risk optimization procedure in the proton treatment planning process and created ROPT plans for a representative prostate

cancer patient using multiple risk models. When the risk model that accounted for initiation, inactivation, repopulation, and promotion (*iirp*) was used, we found that using a combination of anterior and lateral-opposed beams reduced the risk by 21% in the bladder and 30% in the rectum when compared to the current standard of care of lateral-opposed beams alone. We also found that the same anterior and lateral-opposed beam plan reduced the risk by 19% in the bladder and 34% in the rectum for the linear-exponential risk model with the lower level of maximum risk (10 Sv). For all other risk models (linear-non-threshold risk model, both linear plateau risk models, and the linear-exponential risk model with the higher level of maximum risk (40 Sv)) the standard of care plan of lateral-opposed beams provided the lowest total risk and met the objectives to minimize acute toxicity.

The results of this study are of potential clinical significance for several reasons. Others have investigated minimizing risk through choice of treatment modality (Miralbell *et al* 2002, Mu *et al* 2005, Schneider *et al* 2006, Fontenot *et al* 2009, Newhauser *et al* 2009, Bednarz *et al* 2010), reduction of stray radiation exposures due to leakage radiation (Tayama *et al* 2006, Taddei *et al* 2008, Brenner *et al* 2009), optimization of prescription dose (Brodin *et al* 2014), or optimizing treatment plans for a metric other than absorbed dose, such as RBE (Wilkens and Oelfke 2005), linear energy transfer (Grassberger *et al* 2011), robustness (Cao *et al* 2012), or equivalent uniform dose and other radiobiological metrics (Brahme 1999, Wu *et al* 2002, Choi and Deasy 2002, Thieke *et al* 2003, Thomas *et al* 2005, Penagaricano *et al* 2005, Kim and Tomé 2006, Widesott *et al* 2008, Semenenko *et al* 2008, Qi *et al* 2009, Mihaylov *et al* 2011). There has also been progress on integrating risk predictions into the TPS for direct analysis (Hartmann and Schneider 2014). However, ours is the first study to demonstrate algorithmically optimized treatment planning specifically for second cancer risk while maintaining the dose to the tumor. Future studies could apply risk-optimized treatment planning to other, more anatomically complex treatment sites, such as the head and neck, where an algorithmically risk-optimized treatment plan would likely reduce the predicted risk of second cancer compared with plans prepared according to current standards of care which do not yet include risk of second cancer in the optimization process.

The data in the literature that most closely relates to this study is from the work of Fontenot *et al* (2009). It can be estimated from figure 5 of their manuscript that the combined *ERR* to in-field organs following proton therapy for prostate cancer ranges from approximately 1 to 6, depending on risk model (linear-exponential-10 at the low end and linear-non-threshold at the high end), compared with 0.53 to 7.53 in this work. Considering the difference in methods, namely, the use bladder and rectum contours with or without including the contents for risk prediction, our results agree very well. Furthermore, in our previous study (Rechner *et al* 2012), we reanalyzed their data using the same bladder wall and rectal wall contours used in our study and found that the *ERR* from therapeutic radiation for a lateral parallel- opposed treatment would be 7.45 for the linear-non-threshold risk model. This agrees even more closely with the value of 7.53 for the combined *ERR* for second cancer in the bladder and rectum found in this study.

A limitation of this work is the uncertainty in the relationship between dose and risk of second cancer, especially the extent of nonlinearities in the dose-risk relationships. There are

many proposed risk models, such as proposed by Shuryak *et al* (2009a, 2009b, 2011) (used in this study) and Schneider *et al* (2011) that may be particularly appropriate risk models for risk of second cancer following fractionated radiotherapy, since they incorporate both biological parameters and epidemiological data. However, there are currently still large uncertainties with these risk models. We dealt with this uncertainty by performing sensitivity tests to quantify the effects of nonlinearities and other model characteristics. Specifically, we applied a variety of plausible risk models that span the likely relationships between dose and risk of second cancer. What we found in our study is that the qualitative findings from the linear-exponential-40 and both linear-plateau models agree with those from the linear-non-threshold model when DVH constraints were applied. The epidemiological work of Berrington de Gonzalez *et al* (2011) suggests that the organs considered in this study likely follow a linear relationship with dose and risk and that the only organ with clear evidence for a non-linear relationship is the thyroid. If it is true that the risk of second cancer for the bladder and rectum follows a linear (or semi-linear) relationship, a lateral-opposed beam pair provides the lowest predicted risk of second cancer after proton radiotherapy for prostate cancer for the patient studied. However, if future research reveals that the true relationship between dose and carcinogenesis risk would more closely follow the *iirp* or linear-exponential-10 models, the proton treatment plan with the lowest predicted risk of second cancer in the bladder and rectum that also meets acute toxicity constraints is the combination of an anterior beam and a lateral parallel-opposed pair. We would also like to stress that clinical decision making based on risk predictions should only be performed after risk models have been validated, which is outside the scope of this work.

Another limitation of this work is that we only considered the risk of second cancers in the organs from which we expected the largest contribution to predicted risk (the bladder and rectum) and excluded risk of cancer in the bone marrow, soft tissue (sarcoma), skin, and other more distant organs. Furthermore, we did not compare absolute risks nor estimate severities of cancer in the different organs at risk. Future research could include whole-body risk optimization, including estimation of severities for each risk endpoint and, perhaps, patient- or physician-guided prioritization of endpoints. In addition, only one patient was studied in this work. It should be noted that the ROPT plans presented in this study are patient-specific and differences in patient anatomy could yield a different optimal plan.

One of the major strengths of this study is the level of detail of the dose reconstructions. Doses were reconstructed on patient-specific pelvic anatomy, and included simulations of both therapeutic and stray neutron dose, using facility- and patient-specific machine settings. While complete patient-specific neutron dose simulations provided value in this study, an alternative would be to use an analytical model (Zhang *et al* 2010) in a clinical setting where speed is a necessity. Another strength of this study is that the search for the optimal plan was comprehensive. By analyzing risks for all combinations of beam weighting, our approach was immune to being trapped in local minima and potentially missing the global minimum. Future work could include utilization of a different algorithm, for example the conjugate gradient method, which might enable ROPT for very large problem sizes such as intensity-

modulated proton therapy. However, care would need to be taken to ensure the identification of the global minimum.

In conclusion, this study demonstrated that risk-optimized treatment planning is feasible for proton therapy. We found that the optimal treatment plan to reduce the predicted risk of second cancer for a prostate cancer patient depended on the risk model. Future development will be needed to validate risk models, implement these methods clinically, to extend them to optimize other late effects (Zhang *et al* 2013, Pérez-Andújar *et al* 2013, Brodin *et al* 2014), and to consider additional host and treatment related factors.

Acknowledgments

We would like to express our gratitude to Drs. Kenneth Homann, Rajat Kudchadker, Lei Dong, Annelise Giebeler, and Phillip Taddei for valuable discussions and Ms. K. Carnes for assistance in preparing and editing this manuscript. This work was funded in part by grants from the National Cancer Institute (awards 1 R01 CA131463-01A1), the National Institute of Health (award K07CA131505), and Northern Illinois University (subcontract of Department of Defense award W81XWH-08-1-0205).

References

Arvold ND, Niemierko A, Broussard GP, Adams J, Fullerton B, Loeffler JS, Shih HA. Projected second tumor risk and dose to neurocognitive structures after proton versus photon radiotherapy for benign meningioma. Int. J. Radiat. Oncol. Biol. Phys. 2012; 83

Bednarz B, Athar B, Xu XG. A comparative study on the risk of second primary cancers in out of-field organs associated with radiotherapy of localized prostate carcinoma using Monte Carlo-based accelerator and patient models. Med. Phys. 2010; 37:1987–94. [PubMed: 20527532]

Berrington de Gonzalez A, Curtis RE, Kry SF, Gilbert E, Lamart S, Berg CD, Stovall M, Ron E. Proportion of second cancers attributable to radiotherapy treatment in adults: A cohort study in the US SEER cancer registries. Lancet Oncol. 2011; 12:353–60. [PubMed: 21454129]

Brahme A. Optimized radiation therapy based on radiobiological objectives. Semin. Radiat. Oncol. 1999; 9:35–47. Online: http://www.sciencedirect.com/science/article/pii/S1053429699800538. [PubMed: 10196397]

Brenner DJ, Elliston CD, Hall EJ, Paganetti H. Reduction of the secondary neutron dose in passively scattered proton radiotherapy, using an optimized pre-collimator/collimator. Phys. Med. Biol. 2009; 54:6065. Online: http://stacks.iop.org/0031-9155/54/i=20/a=003. [PubMed: 19779218]

Brodin NP, Munck Af, Rosenschöld P, Aznar MC, Kiil-Berthelsen A, Vogelius IR, Nilsson P, Lannering B, Björk-Eriksson T. Radiobiological risk estimates of adverse events and secondary cancer for proton and photon radiation therapy of pediatric medulloblastoma. Acta Oncol. 2011; 50:806–16. Online: http://www.ncbi.nlm.nih.gov/pubmed/21767178. [PubMed: 21767178]

Brodin NP, Vogelius IR, Björk-Eriksson T, Munck Af, Rosenschöld P, Maraldo MV, Aznar MC, Specht L, Bentzen SM. Optimizing the radiation therapy dose prescription for pediatric medulloblastoma: minimizing the life years lost attributable to failure to control the disease and late complication risk. Acta Oncol. 2014; 53:462–70. Online: http://informahealthcare.com/doi/abs/10.3109/0284186X.2013.858824#.U4L2RKhkYEs.mendeley. [PubMed: 24274390]

Cao W, Lim GJ, Lee A, Li Y, Liu W, Ronald Zhu X, Zhang X. Uncertainty incorporated beam angle optimization for IMPT treatment planning. Med. Phys. 2012; 39:5248–56. Online: http://www.pubmedcentral.nih.gov/articlerender.fcgi?artid=3422361&tool=pmcentrez&rendertype=abstract. [PubMed: 22894449]

Choi B, Deasy JO. The generalized equivalent uniform dose function as a basis for intensity-modulated treatment planning. Phys. Med. Biol. 2002; 47:3579–89. [PubMed: 12433121]

Davis RH. 2004 Production and killing of second cancer precursor cells in radiation therapy: in regard to Hall and Wuu (Int J Radiat Oncol Biol Phys 2003;56:83-88). Int. J. Radiat. Oncol. Biol. Phys. 59:916. Online: http://www.sciencedirect.com/science/article/pii/S0360301603020194. [PubMed: 15183501]

Desantis CE, Lin CC, Mariotto AB, Siegel RL, Stein KD, Kramer JL, Alteri R, Robbins AS, Jemal A. 2014 Cancer Treatment and Survivorship Statistics. 2014

Diallo I, Haddy N, Adjadj E, Samand A, Quiniou E, Chavaudra J, Alziar I, Perret N, Guérin S, Lefkopoulos D, de Vathaire F. Frequency distribution of second solid cancer locations in relation to the irradiated volume among 115 patients treated for childhood cancer. Int. J. Radiat. Oncol. Biol. Phys. 2009; 74:876–83. Online: http://www.sciencedirect.com/science/article/pii/S0360301609001369. [PubMed: 19386434]

Efstathiou JA, Paly JJ, Lu HM, Athar BS, Moteabbed M, Niemierko A, Adams JA, Bekelman JE, Shipley WU, Zietman AL, Paganetti H. Adjuvant radiation therapy for early stage seminoma: Proton versus photon planning comparison and modeling of second cancer risk. Radiother. Oncol. 2012; 103:12–7. [PubMed: 22391053]

Followill D, Geis P, Boyer A. Estimates of whole-body dose equivalent produced by beam intensity modulated conformal therapy. Int. J. Radiat. Oncol. 1997; 38:667–72. Online: http://www.sciencedirect.com/science/article/pii/S0360301697000126.

Fontenot JD, Bloch C, Followill D, Titt U, Newhauser WD. Estimate of the uncertainties in the relative risk of secondary malignant neoplasms following proton therapy and intensity-modulated photon therapy. Phys. Med. Biol. 2010; 55:6987–98. [PubMed: 21076196]

Fontenot JD, Lee AK, Newhauser WD. Risk of Secondary Malignant Neoplasms From Proton Therapy and Intensity-Modulated X-Ray Therapy for Early-Stage Prostate Cancer. Int. J. Radiat. Oncol. Biol. Phys. 2009; 74:616–22. [PubMed: 19427561]

Friedman DL, Whitton J, Leisenring W, Mertens AC, Hammond S, Stovall M, Donaldson SS, Meadows AT, Robison LL, Neglia JP. Subsequent neoplasms in 5-year survivors of childhood cancer: The childhood cancer survivor study. J. Natl. Cancer Inst. 2010; 102:1083–95. [PubMed: 20634481]

Grassberger C, Trofimov A, Lomax A, Paganetti H. Variations in linear energy transfer within clinical proton therapy fields and the potential for biological treatment planning. Int. J. Radiat. Oncol. Biol. Phys. 2011; 80:1559–66. [PubMed: 21163588]

Hartmann M, Schneider U. Integration of second cancer risk calculations in a radiotherapy treatment planning system. J. Phys. Conf. Ser. 2014; 489:012049. Online: http://stacks.iop.org/1742-6596/489/i=1/a=012049?key=crossref.97b67ca1e18e47c384039872adb1b541.

ICRP. ICRP Publication 110: Adult reference computational phantoms. Ann. ICRP. 2008; 39:1–165. Online: http://linkinghub.elsevier.com/retrieve/pii/S0146645309000311.

ICRU. Prescribing, Recording, and Reporting Proton-Beam Therapy. J. Int. Comm. Radiat. Units Meas. Int. At. Energy Agency. 2007. **Report 78** Online: http://www.icru.org/home/reports/prescribing-recording-and-reporting-proton-beam-therapy-icru-report-78

Kim Y, Tomé W a. Risk-adaptive optimization: selective boosting of high-risk tumor subvolumes. Int. J. Radiat. Oncol. Biol. Phys. 2006; 66:1528–42. Online: http://www.pubmedcentral.nih.gov/articlerender.fcgi?artid=2423330&tool=pmcentrez&rendertype=abstract. [PubMed: 17126211]

Lindsay, K a; Wheldon, EG.; Deehan, C.; Wheldon, TE. Radiation carcinogenesis modelling for risk of treatment-related second tumours following radiotherapy. Br. J. Radiol. 2001; 74:529–36. Online: http://www.birpublications.org/doi/abs/10.1259/bjr.74.882.740529. [PubMed: 11459732]

Mihaylov, IB.; Fatyga, M.; Bzdusek, K.; Gardner, K.; Moros, EG. Biological Optimization in Volumetric Modulated Arc Radiotherapy for Prostate Carcinoma.; Int. J. Radiat. Oncol. Biol. Phys. 2011. p. 1-7.Online: http://www.ncbi.nlm.nih.gov/pubmed/21570214

Miralbell R, Lomax A, Cella L, Schneider U. Potential reduction of the incidence of radiation-induced second cancers by using proton beams in the treatment of pediatric tumors. 2002; 54

Moteabbed M, Yock TI, Paganetti H. The risk of radiation-induced second cancers in the high to medium dose region: a comparison between passive and scanned proton therapy, IMRT and VMAT for pediatric patients with brain tumors. Phys. Med. Biol. 2014; 59:2883–99. Online: http://www.ncbi.nlm.nih.gov/pubmed/24828559. [PubMed: 24828559]

Moyers MF, Miller DW, Bush DA, Slater JD. Methodologies and tools for proton beam design for lung tumors. Int. J. Radiat. Oncol. 2001; 49:1429–38. Online: http://www.sciencedirect.com/science/article/pii/S0360301600015558.

Mu X, Björk-Eriksson T, Nill S, Oelfke U, Johansson K-A, Gagliardi G, Johansson L, Karlsson M, Zackrisson DB. Does electron and proton therapy reduce the risk of radiation induced cancer after spinal irradiation for childhood medulloblastoma? A comparative treatment planning study. Acta Oncol. 2005; 44:554–62. [PubMed: 16165914]

NCRP. Second Primary Cancers and Cardiovascular Disease After Radiation Therapy. Natl. Counc. Radiat. Prot. Meas. 2011:1–375. Report 170.

Newhauser WD, Durante M. Assessing the risk of second malignancies after modern radiotherapy. Nat. Rev. Cancer. 2011; 11:438–48. Online: http://www.ncbi.nlm.nih.gov/pubmed/21593785. [PubMed: 21593785]

Newhauser WD, Fontenot JD, Mahajan A, Kornguth D, Stovall M, Zheng Y, Taddei PJ, Mirkovic D, Mohan R, Cox JD, Woo S. The risk of developing a second cancer after receiving craniospinal proton irradiation. Phys. Med. Biol. 2009; 54:2277–91. [PubMed: 19305036]

Newhauser W, Fontenot J, Zheng Y, Polf J, Titt U, Koch N, Zhang X, Mohan R. Monte Carlo simulations for configuring and testing an analytical proton dose-calculation algorithm. Phys. Med. Biol. 2007; 52:4569–84. [PubMed: 17634651]

NRC. National Research Council BEIR VII: Health Risks From Exposure to Low Levels of Ionizing Radiation. The National Academies Press; Washington D.C.: 2006.

Penagaricano JA, Papanikolaou N, Wu C, Yan Y. An assessment of Biologically-based Optimization (BORT) in the IMRT era. Med. Dosim. 2005; 30:12–9. [PubMed: 15749006]

Pérez-Andújar A, Newhauser WD, Taddei PJ, Mahajan A, Howell RM. The predicted relative risk of premature ovarian failure for three radiotherapy modalities in a girl receiving craniospinal irradiation. Phys. Med. Biol. 2013; 58:3107–23. Online: http://www.pubmedcentral.nih.gov/articlerender.fcgi?artid=3875375&tool=pmcentrez&rendertype=abstract. [PubMed: 23603657]

Qi XS, Semenenko VA, Li XA. Improved critical structure sparing with biologically based IMRT optimization. Med. Phys. 2009; 36:1790–9. [PubMed: 19544798]

Rechner, L a; Howell, RM.; Zhang, R.; Etzel, C.; Lee, AK.; Newhauser, WD. Risk of radiogenic second cancers following volumetric modulated arc therapy and proton arc therapy for prostate cancer. Phys. Med. Biol. 2012; 57:7117–32. Online: http://www.pubmedcentral.nih.gov/articlerender.fcgi?artid=3772654&tool=pmcentrez&rendertype=abstract. [PubMed: 23051714]

Sachs RK, Brenner DJ. Solid tumor risks after high doses of ionizing radiation. Proc. Natl. Acad. Sci. U. S. A. 2005; 102:13040–5. Online: http://www.pnas.org/cgi/content/long/102/37/13040. [PubMed: 16150705]

Schneider U, Lomax A, Pemler P, Besserer J, Ross D, Lombriser N, Kaser-Hotz B. The impact of IMRT and proton radiotherapy on secondary cancer incidence. Strahlentherapie und Onkol. 2006; 182:647–52.

Schneider U, Sumila M, Robotka J. Site-specific dose-response relationships for cancer induction from the combined Japanese A-bomb and Hodgkin cohorts for doses relevant to radiotherapy. Theor. Biol. Med. Model. 2011; 8:27. Online: http://www.pubmedcentral.nih.gov/articlerender.fcgi?artid=3161945&tool=pmcentrez&rendertype=abstract. [PubMed: 21791103]

Schneider U, Walsh L. Cancer risk estimates from the combined Japanese A-bomb and Hodgkin cohorts for doses relevant to radiotherapy. Radiat. Environ. Biophys. 2008; 47:253–63. Online: http://www.ncbi.nlm.nih.gov/pubmed/18157543. [PubMed: 18157543]

Semenenko VA, Reitz B, Day E, Qi XS, Miften M, Li XA. Evaluation of a commercial biologically based IMRT treatment planning system. Med. Phys. 2008; 35:5851–60. [PubMed: 19175141]

Shuryak I, Hahnfeldt P, Hlatky L, Sachs RK, Brenner DJ. A new view of radiation-induced cancer: integrating short- and long-term processes. Part I: approach. Radiat. Environ. Biophys. 2009a; 48:263–74. Online: http://www.pubmedcentral.nih.gov/articlerender.fcgi?artid=2714893&tool=pmcentrez&rendertype=abstract. [PubMed: 19536557]

Shuryak I, Hahnfeldt P, Hlatky L, Sachs RK, Brenner DJ. A new view of radiation-induced cancer: integrating short- and long-term processes. Part II: second cancer risk estimation. Radiat. Environ. Biophys. 2009b; 48:275–86. Online: http://www.pubmedcentral.nih.gov/articlerender.fcgi?artid=2714894&tool=pmcentrez&rendertype=abstract. [PubMed: 19499238]

Shuryak I, Hahnfeldt P, Hlatky L, Sachs RK, Brenner DJ. Erratum to: A new view of radiation-induced cancer: integrating short- and long-term processes. Parts I and II. Radiat. Environ. Biophys. 2011; 50:607–8. Online: http://link.springer.com/10.1007/s00411-011-0378-5.

Siegel R, Ma J, Zou Z, Jemal A. Cancer statistics, 2014. CA Cancer J Clin. 2014; 64:9–29. Online: http://www.ncbi.nlm.nih.gov/pubmed/24399786. [PubMed: 24399786]

Taddei PJ, Fontenot JD, Zheng Y, Mirkovic D, Lee AK, Titt U, Newhauser WD. Reducing stray radiation dose to patients receiving passively scattered proton radiotherapy for prostate cancer. Phys. Med. Biol. 2008; 53:2131. Online: http://stacks.iop.org/0031-9155/53/i=8/a=009. [PubMed: 18369278]

Taddei PJ, Howell RM, Krishnan S, Scarboro SB, Mirkovic D, Newhauser WD. Risk of second malignant neoplasm following proton versus intensity-modulated photon radiotherapies for hepatocellular carcinoma. Phys. Med. Biol. 2010; 55:7055–65. [PubMed: 21076199]

Tayama R, Fujita Y, Tadokoro M, Fujimaki H, Sakae T, Terunuma T. Measurement of neutron dose distribution for a passive scattering nozzle at the Proton Medical Research Center (PMRC). Nucl. Instruments Methods Phys. Res. Sect. A Accel. Spectrometers, Detect. Assoc. Equip. 2006; 564:532–6. Online: http://www.sciencedirect.com/science/article/pii/S016890020600636X.

Thieke C, Bortfeld T, Niemierko A, Nill S. From physical dose constraints to equivalent uniform dose constraints in inverse radiotherapy planning. Med. Phys. 2003; 30:2332–9. [PubMed: 14528955]

Thomas E, Chapet O, Kessler ML, Lawrence TS, Ten Haken RK. Benefit of using biologic parameters (EUD and NTCP) in IMRT optimization for treatment of intrahepatic tumors. Int. J. Radiat. Oncol. Biol. Phys. 2005; 62:571–8. [PubMed: 15890602]

Verellen D, Vanhavere F. Risk assessment of radiation-induced malignancies based on whole-body equivalent dose estimates for IMRT treatment in the head and neck region. Radiother. Oncol. 1999; 53:199–203. Online: http://www.sciencedirect.com/science/article/pii/S0167814099000791. [PubMed: 10660198]

Widesott L, Strigari L, Pressello MC, Benassi M, Landoni V. Role of the parameters involved in the plan optimization based on the generalized equivalent uniform dose and radiobiological implications. Phys. Med. Biol. 2008; 53:1665–75. [PubMed: 18367795]

Wilkens JJ, Oelfke U. Optimization of radiobiological effects in intensity modulated proton therapy. Med. Phys. 2005; 32:455–65. [PubMed: 15789592]

Wu Q, Mohan R, Niemierko A, Schmidt-Ullrich R. Optimization of intensity-modulated radiotherapy plans based on the equivalent uniform dose. Int. J. Radiat. Oncol. Biol. Phys. 2002; 52:224–35. [PubMed: 11777642]

Zhang R, Howell RM, Homann K, Giebeler A, Taddei PJ, Mahajan A, Newhauser WD. Predicted risks of radiogenic cardiac toxicity in two pediatric patients undergoing photon or proton radiotherapy. Radiat. Oncol. 2013; 8:184. Online: http://www.pubmedcentral.nih.gov/articlerender.fcgi?artid=3751146&tool=pmcentrez&rendertype=abstract. [PubMed: 23880421]

Zhang R, Pérez-Andújar A, Fontenot JD, Taddei PJ, Newhauser WD. An analytic model of neutron ambient dose equivalent and equivalent dose for proton radiotherapy. Phys. Med. Biol. 2010; 55:6975–85. [PubMed: 21076197]

Zheng Y, Fontenot J, Taddei P, Mirkovic D, Newhauser W. Monte Carlo simulations of neutron spectral fluence, radiation weighting factor and ambient dose equivalent for a passively scattered proton therapy unit. Phys. Med. Biol. 2008; 53:187–201. [PubMed: 18182696]

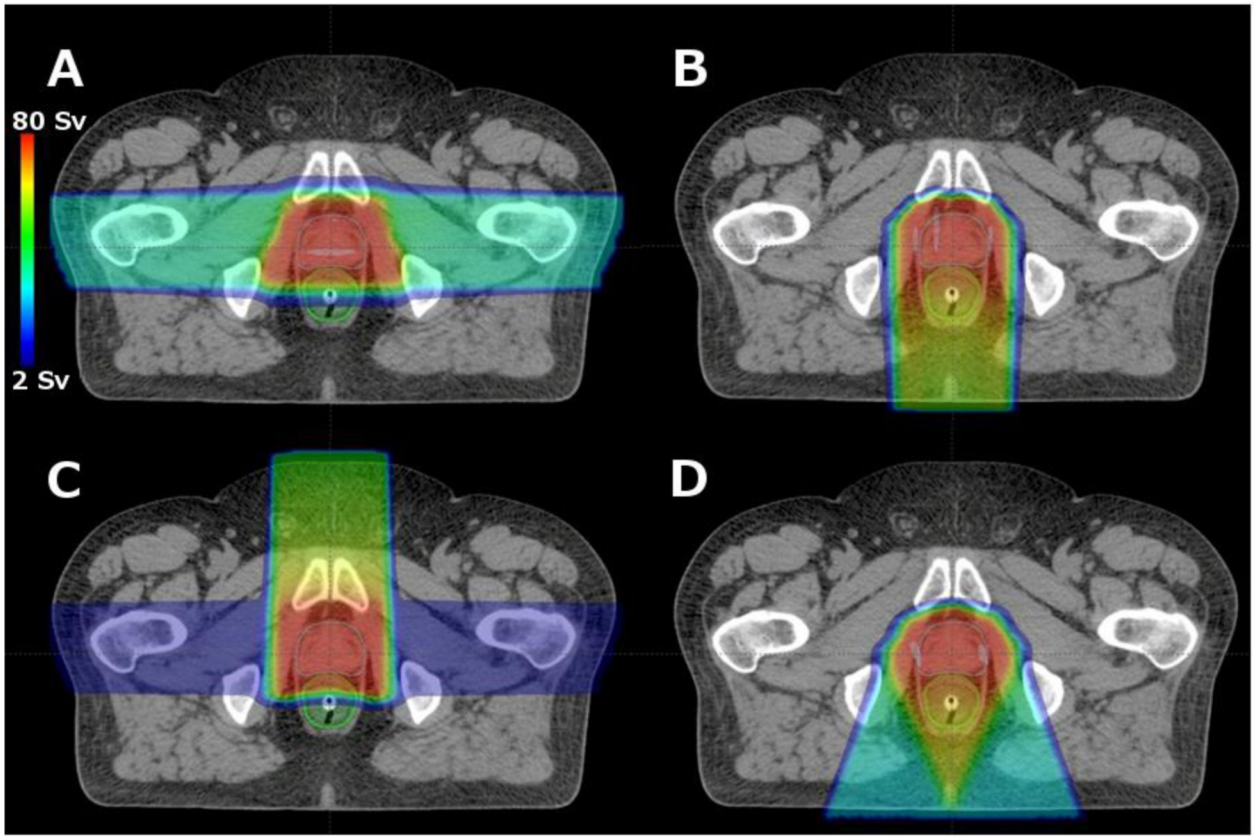

Figure 1.

Axial slice showing risk-optimized proton therapy (ROPT) treatment plans with and without DVH constraints applied during the planning process for 6 different risk models, which yielded only 4 unique plans (A-D). Specific details regarding plans A-D are listed in tables 4 and 5. In general, Plan A was selected using the linear non-threshold risk model and met all DVH constraints for normal tissue. Plans B and D were selected using risk models that assumed decreased risk at high doses due to inactivation, but did not meet the DVH constraints. When DVH constraints were considered for these models, Plan C was selected as the compromise between acute toxicity and risk of second cancer.

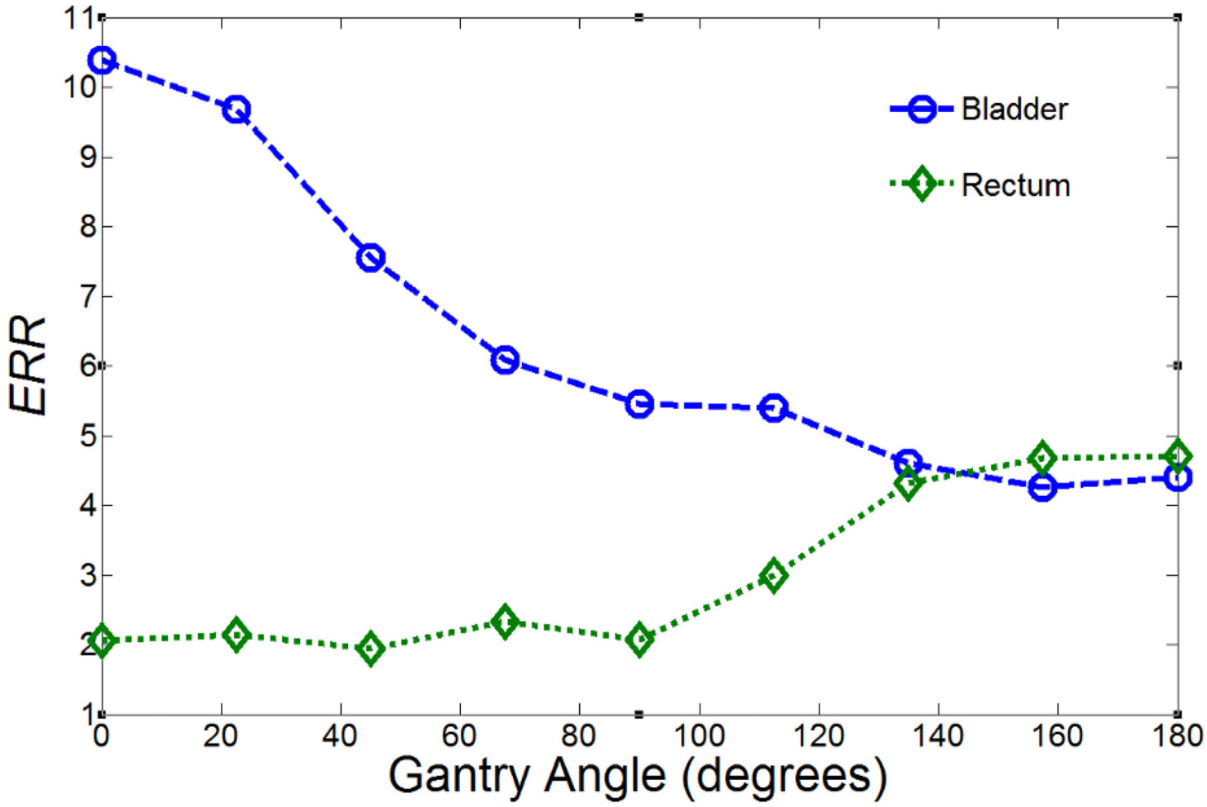

Figure 2.

Predicted excess relative risk (*ERR*) versus beam angle (θ) for second cancer in the bladder and rectum using the linear-non-threshold risk model. *ERR* values are the average of the values from the left and right corresponding beam angles (the beam angle listed and the contralateral beam mirrored over the sagittal axis) because of the symmetry of the pelvic anatomy. For this figure, the beam weight for the angle of interest is set to 1, with all other beam weights set to 0.

Table 1

Dose volume histogram (DVH) constraints used clinically at our institution (units of Gy) and for this study (units of Sv), where the tissue should receive no greater than the dose specified to the volume of tissue specified.

Normal Tissue	Dose (Gy or Sv)	Percent Volume (%)
Rectum	40	60
	45	50
	60	40
	70	15
	75.6	10
	78	5
Bladder	70	15
Rectal Wall	60	70
79	30	
Femoral Heads	45	50

Table 2

Parameters and their assumed values in the *iirp* risk model in our study (Shuryak *et al* 2009a, 2009b, 2011). Indices *i* and *k* denote the *i*th voxel and *k*th fraction. If the value column is left empty, that signifies that the value varies with voxel or fraction. If two values are listed, the first corresponds to the bladder and the second corresponds to the rectum.

Parameter	Value	Unit	Definition
N		voxels	Number of voxels in a tissue
V_i		cc	Volume of a voxel
V_t		cc	Volume of a tissue
Y	0.626, 0.0717	Sv^{-1}	Characterizes the dose-dependency of promotion
X	0.151, 2.40	years/Sv	Characterizes the dose-dependency of initiation
δ	1.68, 0.0193	10^{-3} $years^{-1}$	Describes homeostatic regulation of the number of pre-malignant stem cells per niche
b	0.282, 0.217	$years^{-1}$	Pre-malignant niche replication rate
T_y	10	years	Time since exposure
T_x	60	years	Age at exposure
D(i)		Sv	Total dose for all fractions to a given voxel
d(i,k)		Sv	Fraction dose to a given voxel
K	38	fractions	Number of fractions
I(i,k)		Sv	Helps to describe the number of cells initiated
F(i,k)		-	Clone survival probability
v	602.6, 251.2	cells	Number of stem cells present before irradiation
$n-^{or+}(i,k)$		cells	Normal stem cell number before (-) and after (+) fraction
S(i,k)		-	Surviving fraction of cells
Z	602.6, 251.2	cells/niche	Carrying capacity for pre-malignant stem cells per niche
α	0.25	Sv^{-1}	Stem cell radiation inactivation constant
β	0.025	Sv^{-2}	Stem cell radiation inactivation constant
λ	0.05, 0.10	$time^{-1}$	Maximum net proliferation rate (repopulation)
n-(K+1)	v	cells	Number of stem cells at large time after exposure
F(K)	1	-	Clone survival probability after last fraction

Table 3

Tissue-specific risk parameters for second cancer induction 10 years after exposure at 60 years of age for the other 5 risk models.

		Linear-non-threshold	Linear-exponential-10	Linear-exponential-40	Linear-plateau-10	Linear-plateau-40
μ_T	Bladder	0.40	0.49	0.46	0.51	0.47
	Colon	0.51	0.61	0.57	0.65	0.58
α_T	Bladder	-	0.09	0.025	0.25	0.068
	Colon	-	0.09	0.025	0.25	0.068

Table 4

Details describing risk-optimized proton therapy (ROPT) treatment plans for prostate radiotherapy. Results were obtained without normal tissue DVH constraints for linear and non-linear risk models. Axial slices of the treatment plans are shown in figure 1.

	Without DVH Constraints					
Risk model	**Plan description**	**Gantry Angles (degrees)**	**Beam Weights**	$ERR_{bladder}$	ERR_{rectum}	**Plan Label**
iirp (Shuryak *et al*)	Posterior	180	1	0.52	0.10	B
Linear-non-threshold	Lateral parallel-opposed	90, 270	0.5, 0.5	5.46	2.07	A
Linear-exponential-10	Posterior	180	1	0.21	0.06	B
Linear-exponential-40	Posterior oblique	157.5, 202.5	0.5, 0.5	1.08	0.96	D
Linear-plateau-10	Posterior oblique	157.5, 202.5	0.5, 0.5	0.49	0.39	D
Linear-plateau-40	Lateral parallel-opposed	90, 270	0.5, 0.5	1.74	0.65	A

Table 5

Results from risk optimization, describing which treatment plan confers the lowest predicted risk of second cancer following prostate radiotherapy. Results were obtained with normal tissue DVH constraints for linear and non-linear risk models. Axial slices of the treatment plans are shown in figure 1.

	With DVH Constraints					
Risk model	**Plan description**	**Gantry Angles (degrees)**	**Beam Weights**	$ERR_{bladder}$	ERR_{rectum}	**Plan Label**
iirp (Shuryak *et al*)	Anterior and Lateral parallel-opposed	0, 90, 270	0.9, 0.05, 0.05	0.73	0.14	C
Linear-non-threshold	Lateral parallel-opposed	90, 270	0.5, 0.5	5.46	2.07	A
Linear-exponential-10	Anterior and Lateral parallel-opposed	0, 90, 270	0.9, 0.05, 0.05	0.32	0.09	C
Linear-exponential-40	Lateral parallel-opposed	90, 270	0.5, 0.5	1.54	0.59	A
Linear-plateau-10	Lateral parallel-opposed	90, 270	0.5, 0.5	0.74	0.27	A
Linear-plateau-40	Lateral parallel-opposed	90, 270	0.5, 0.5	1.74	0.65	A